



Cite this: *Environ. Sci.: Nano*, 2019, 6, 2767

The heterogeneous reaction of dimethylamine/ammonia with sulfuric acid to promote the growth of atmospheric nanoparticles†

Weina Zhang, Yuemeng Ji, Guiying Li,  Qiuju Shi and Taicheng An *

The growth of atmospheric nanoparticles plays key roles in a new particle formation (NPF) event. However, the interface heterogeneous reaction mechanism of dimethylamine (DMA)/ammonia with sulfuric acid (SA) to promote the growth of atmospheric nanoparticles remains unclear. In this work, an atmospheric nanoparticle model with 59 wt% SA was constructed, and the heterogeneous reactions of DMA/ammonia with SA in the air–nanoparticle interface as well as inside the bulk nanoparticle were comparably investigated with theoretical methods. The results revealed that the interface reaction mechanism of DMA to promote atmospheric nanoparticle growth is different from that of ammonia. DMA more readily approaches the air–nanoparticle interface than ammonia, which is more conducive to the occurrence of the heterogeneous reaction of DMA with SA in the interface than that of ammonia. In the DMA–SA–water system, the first solvation shell is composed of SA and water when DMA approaches the air–nanoparticle interface, and the DMA–SA cluster is subsequently formed in the air–aerosol interface. Accordingly, the efficiency of DMA in facilitating aerosol growth is independent from the concentration of gaseous SA. Moreover, DMA is more competitive in promoting the growth of concentrated aerosol than ammonia. In contrast, in the ammonia–SA–water system, the first solvation shell is re-composed of SA and water when ammonia is dissolved into the bulk nanoparticle, and the ammonia–SA cluster is formed. Furthermore, the growth of the nanoparticle depends on the concentration of gaseous SA. Considering the 2–3 orders of magnitude higher concentration of ammonia than DMA in the atmosphere, the growth of fresh aerosol is more easily promoted by ammonia than DMA. The conclusion that the growth of the nanoparticle was gradually promoted by the acidity of the first formed DMA–SA cluster during the NPF events was also obtained.

Received 3rd June 2019,
Accepted 18th July 2019

DOI: 10.1039/c9en00619b

rscl.li/es-nano

Environmental significance

The key steps in a new particle formation (NPF) event include formation and growth of the nanoparticle. The heterogeneous reaction of dimethylamine (DMA)/ammonia with SA contributes to the growth of the nanoparticle. However, the mechanism of the heterogeneous reaction remains unclear. Furthermore, experimental methods could not differentially probe the region of the air–nanoparticle interface from the region of the bulk nanoparticle. Complementary to experimental methods, this work mainly applied theoretical methods for investigating the heterogeneous reaction of DMA/ammonia to promote the growth of the nanoparticle. The results confirmed that the DMA–SA reaction proceeds in the air–nanoparticle interface, while the ammonia–SA reaction proceeds inside the bulk nanoparticle. Hence, DMA is more competitive in promoting the growth of a concentrated nanoparticle. The growth of a fresh nanoparticle is more promoted by ammonia considering the higher concentration of ammonia than that of DMA in the atmosphere. It is further speculated that DMA would promote the sustainable growth of an acid nanoparticle as the acidity is gradually concentrated during the NPF events.

1. Introduction

New particle formation (NPF) has significant impacts on regional and global climates, air quality, and human

health.^{1–3} Overall assessments of these impacts require detailed information of how nanoparticles were formed and grown in the atmospheric interface. The key steps in NPF include formation and growth of nanoparticles,⁴ and sulfuric acid (SA) has been recognized as a base species for nanoparticle formation.^{5,6} However, the SA–water binary theory cannot explain most of the NPF events in the boundary layer at the present stage.⁷ The discrepancies in NPF rates between models and experimental observations suggest that other potential reactions with other species, such as amines and ammonia, are also involved.^{4,8,9}

Guangzhou Key Laboratory of Environmental Catalysis and Pollution Control, Guangdong Key Laboratory of Environmental Catalysis and Health Risk Control, School of Environmental Science and Engineering, Institute of Environmental Health and Pollution control, Guangdong University of Technology, Guangzhou 510006, China. E-mail: antc99@gdut.edu.cn

† Electronic supplementary information (ESI) available. See DOI: 10.1039/c9en00619b

Amines and ammonia are strong base species that neutralize SA in the atmosphere; nevertheless amines are believed to be stronger than ammonia in promoting the growth of nanoparticles from field observation and experimental evidence.^{10–12} For instance, a DMA–SA–water cluster was observed to coincide with high NPF rates in mega cities,¹² although the concentration of gaseous amines is 2–3 orders of magnitude lower than that of ammonia in the atmosphere.¹³ In order to explain the higher efficiency of DMA in promoting the growth of nanoparticles than that of ammonia, some experimental studies were carried out in an attempt to clarify the heterogeneous processes of DMA or ammonia uptake by the SA nanoparticle.^{14–17} It is observed that the uptake coefficient of DMA by the SA nanoparticle depends weakly on the concentration of gaseous SA.¹⁶ For another example, in the case of ammonia, the SA nanoparticle with an initial diameter of 45 nm can grow to a larger size at lower relative humidity <5%,¹⁴ while no apparent growth of the SA nanoparticle is observed at higher relative humidity (25% and 75%).¹⁵ The lower humidity is related to the higher concentration of gaseous SA in the atmosphere, thereby the efficiency of ammonia in promoting the growth of the SA nanoparticle depends on the concentration of gaseous SA.¹⁷ The experimental results clarified the distinct difference of DMA from ammonia and more detailed information about the heterogeneous reactions needs to be further obtained.

Heterogeneous reactions play significant roles in the growth of particles.¹⁸ Atmospheric nanoparticles can undergo component modification and growth *via* heterogeneous reactions with DMA^{19–21} or ammonia.^{14,17,22} Previous studies of other species such as volatile organic compounds indicated that the heterogeneous reactions occurring in the air–nanoparticle interface might be different from those in the bulk nanoparticle.^{23–25} However, it is challenging to obtain detailed experimental information of heterogeneous reactions in different regions,^{26,27} because experimental methods could not differentially probe the air–nanoparticle interface from the bulk aqueous phase.²³ Complementary to experimental methods, theoretical methods, such as the molecular dynamics (MD) method and quantum mechanics (QM) method, have the advantage of recording detailed information on different regions of the nanoparticle.²⁸ Most previous theoretical studies focused on the heterogeneous reactions of species approaching the droplet, but studies on the SA nanoparticle are still lacking. Since the SA concentration of the SA nanoparticle could affect the mechanism of DMA/ammonia in promoting nanoparticle growth, a comprehensive understanding of the heterogeneous reactions of DMA/ammonia with SA deserves further elucidation from the point of view of theoretical chemical calculations.

Accordingly, the heterogeneous reactions of DMA/ammonia with SA were investigated in this work using theoretical methods as a supplement to experimental research. For evaluating the influence of the SA component on the reaction mechanism of DMA/ammonia in promoting the growth of nanoparticles, a model nanoparticle composed of SA and wa-

ter was constructed, and the changes in the stability of the DMA/ammonia system were evaluated using the free energy profile. After DMA/ammonia was moved into the air–nanoparticle interface or inside the bulk nanoparticle, the heterogeneous reactions occurring in the two regions were probed in detail, respectively. Furthermore, to understand the mechanism of DMA/ammonia–SA reactions, the DMA/ammonia–SA cluster was extracted from the MD configuration and was re-optimized by the QM method. Based on the obtained results, the environmental implications of the heterogeneous reactions of DMA/ammonia with SA on the promoted growth of nanoparticles were also discussed.

2. Methods

A model nanoparticle composed of water was first constructed, and tests were performed for determining the most appropriate number of water molecules based on the homogeneity and cohesiveness of the ambient droplet. The details of the tests are described in the ESI† (Fig. S1 and S2). Hence, a model containing 577 water molecules within a box of 2.6 nm³ volume was constructed. The size of sub-3 nm is a critical size for a nanoparticle to grow to a few nanometers in an NPF event.¹² Therefore, in this work, a size of 2.6 nm was chosen for the model. The calculated density of the droplet is 1.004 g cm⁻³, which is close to 0.997 g cm⁻³ under ambient conditions.²⁹ An acid aerosol containing 59 wt% SA was constructed based on the droplet model, and the SA concentration was selected according to the lowest value employed in the experimental data.¹⁶ The initial positions of water and SA molecules were determined using the Monte Carlo method and subsequently confirmed using the MD method. 500 ps equilibration was executed in the *NPT* ensemble (*N*, *P* and *T* represent the number of atoms, pressure and temperature, respectively) to guarantee the thermodynamic equilibrium of the acid aerosol. A vacuum layer of 3 nm was added above the acid aerosol in order to avoid disturbances from other mirror images. The DMA/ammonia molecule was placed at a distance of 2.5 nm above the mass center of the aqueous aerosol. The DMA/ammonia–SA–water system was fully equilibrated in the *NPT* ensemble and then sampled in the *NVT* ensemble (*N*, *V* and *T* represent the number of atoms, volume and temperature, respectively). The target temperature and pressure of ambient conditions were controlled at 298 K and 1 bar with a Langevin thermostat and barostat, respectively. Either stage was executed for 100 ps at a timestep of 1 fs. Water was described by the TIP3P model,^{24,30} and DMA, ammonia and SA molecules were described by the CHARMM field.^{31–33} Periodic boundary conditions were employed for three dimensions, and the Lennard-Jones and real space coulombic interactions were cut off at 12.0 Å. The Coulomb term was determined by the Ewald summation method in an accuracy of 0.0001 kcal mol⁻¹. The particle mesh Ewald method was employed with an interpolation order of 6 and a grid spacing of 0.8 Å. 1000 steps of geometry optimization were executed before MD equilibration.

All the geometry optimization and MD calculations were performed with the NAMD package³⁴ and the corresponding dynamical configurations were visualized using VMD software.³⁵

The free energy profile was computed using umbrella sampling³⁶ and the weighted histogram analysis method (WHAM)^{37,38} based on the equilibrated MD trajectories. The reaction coordinate is from the mass center of the acid aerosol to the mass center of DMA/ammonia. The position of DMA/ammonia was varied by a step of 0.1 nm, so that DMA/ammonia was finally moved into the bulk aerosol. The trajectory was carried out for 100 ps at each new position of DMA/ammonia. The bias potential force constant is equal to 10 kcal mol⁻¹ Å⁻².²⁴

In order to confirm the interactions of DMA/ammonia with solutes, the representative configuration response to the equilibrated states of the DMA/ammonia-SA-water system is extracted when DMA or ammonia approaches the surface and the bulk aerosol (Fig. S3 and S4†). For the confirmation of the reaction of DMA/ammonia with SA, the cluster of DMA/ammonia-SA from specific configurations was re-optimized at the M06-2X/6-311G(d,p) level which has been successfully applied in the calculation of atmospheric reactions.^{39,40} The subsequent normal-mode vibrational frequency analysis was performed along the potential energy surface. All the QM calculations were implemented using the Gaussian 09 package.⁴¹

3. Results and discussion

3.1 The heterogeneous process of DMA/ammonia approaching the nanoparticle

During the heterogeneous process, DMA/ammonia is moved along the path from the air to the mass center of the nanoparticle. When DMA/ammonia is initially placed in the air-nanoparticle interface, the occurrence probabilities of SA-water and DMA/ammonia along the path are illustrated in Fig. 1a. The method for calculating the occurrence probability is described in the ESI† which is referenced from Martins-Costa *et al.*'s studies.^{24,42} According to the occurrence probability of SA-water (the black dashed line in Fig. 1a), the local concentration of SA-water dramatically changes in the region of the particle-interface and the region of the interface-air, respectively. Thus, the range of the air-nanoparticle interface is from 6.6 Å to 13.7 Å. The occurrence probabilities of DMA (the red solid line in Fig. 1a) and ammonia (the blue solid line in Fig. 1a) are compared. The moving range of ammonia is from 9.6 Å to 14.7 Å, while the moving range of DMA is from 7.1 Å to 13.7 Å. Thus, the moving ranges of ammonia and DMA are within the range of the air-nanoparticle interface. However, the moving range of DMA is 1.5 Å wider than that of ammonia, indicating that DMA is more likely to easily interact with SA and water in the air-nanoparticle interface than ammonia.

The changes of the stability of the system can be reflected by the free energy profile,^{42,43} and the free energy of the

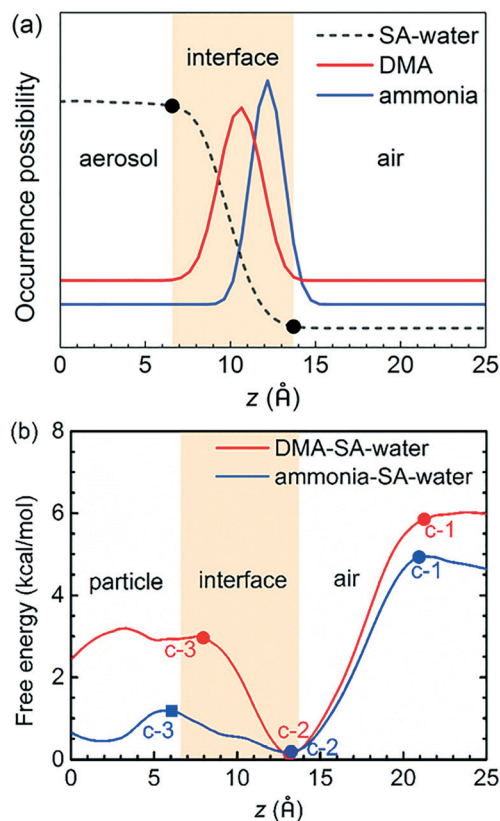


Fig. 1 DMA more easily approaches the air-nanoparticle interface than ammonia: (a) the occurrence probability of DMA (the red solid line), ammonia (the blue solid line), and SA-water (the black dashed line); (b) free energy profiles of the DMA-SA-water system (the red line) and the ammonia-SA-water system (the blue line). The coordinate is set normal to the air-nanoparticle interface (denoted as z), where the origin ($z = 0$) is consistent with the mass center of the nanoparticle. The air-nanoparticle interface is denoted by the yellow box.

DMA/ammonia-SA-water system varies as the changes in the positions of DMA/ammonia as shown in Fig. 1b. There are three special points in the free energy profile: point c-1 corresponds to the first turning point in the air, and indicates that DMA/ammonia starts to be adsorbed by the nanoparticle; point c-2 represents the lowest point in the air/nanoparticle interface, and implies the highest stability of DMA/ammonia interacting with interfacial SA and water; point c-3 denotes the first turning point inside the bulk nanoparticle, and indicates that DMA/ammonia is totally dissolved inside the bulk nanoparticle. DMA can be spontaneously adsorbed onto the air-nanoparticle interface, as the free energy of point c-2 is found to be 5.7 kcal mol⁻¹ lower than that of point c-1 (the red line in Fig. 1b). The DMA-SA-water system presents a higher stability when DMA is in the air-nanoparticle interface than that when DMA is inside the bulk nanoparticle, because the free energy of point c-2 is 2.9 kcal mol⁻¹ lower than that of point c-3. Therefore, DMA more easily facilitates the heterogeneous interactions with SA or water in the air-nanoparticle interface than inside the bulk nanoparticle. This makes it possible for DMA to capture aqueous SA inside the

bulk nanoparticle and gaseous SA from the air simultaneously. In the ammonia-SA-water system (the blue line in Fig. 1b), the free energy of point c-2 is found to be 4.1 kcal mol⁻¹ lower than that of point c-1, implying that ammonia can also be spontaneously adsorbed onto the air-nanoparticle interface. The free energy of point c-2 is 0.6 kcal mol⁻¹ lower than that of point c-3. This indicates the somewhat higher stability of the ammonia-SA-water system when ammonia is in the air-nanoparticle interface than that when ammonia is inside the bulk nanoparticle. However, the free energy difference between point c-2 and point c-3 is less than 1 kcal mol⁻¹; thus it is relatively easy for ammonia to overcome the free energy difference to be dissolved into the bulk nanoparticle.

Moreover, the free energy difference between points c-2 and c-3 in the DMA-SA-water system is 4.8 times the free energy difference from the ammonia-SA-water system, thereby it is more difficult for DMA to enter inside the bulk nanoparticle from the air-nanoparticle interface than ammonia. This may explain the slower heterogeneous process of DMA uptake by the acid aerosol than that of ammonia observed in the experiments.¹⁶ Thus, DMA more readily facilitates the heterogeneous reactions with SA or water in the air-nanoparticle interface than ammonia.

3.2 The heterogeneous reactions in the DMA-SA-water system

The free energy profile of the DMA-SA-water system changes dramatically when DMA is moved from the air-nanoparticle interface to the bulk nanoparticle. It is because the move-

ments of DMA immediately cause changes in the heterogeneous reactions in the DMA-SA-water system. In order to figure out the changes in the heterogeneous reactions, the heterogeneous reactions occurring in the regions of the interface and the bulk particle would be differently probed.

In the air-aqueous interface or aqueous bulk, close interactions between solutes and solutions occur. The first solution shell is thus formed around the specific solute. The components of the first solution shell can be quantified by the coordination numbers. The coordination numbers are calculated as the integrations of RDF within $r = 2.5$ Å. The distance of 2.5 Å is considered as the threshold value to determine whether close interactions occur between two specific atoms. It is also used as the threshold distance in Martins-Costa *et al.*'s study²⁴ where they investigated the heterogeneous interactions of volatile organic compounds with water. Therefore, firstly, four types of hydrogen bonds (HBs) are analyzed: $N_{\text{DMA}} \cdots H_{\text{SA}}$, $H_{\text{DMA}} \cdots O_{\text{SA}}$, $N_{\text{DMA}} \cdots H_{\text{water}}$ and $H_{\text{DMA}} \cdots O_{\text{water}}$. The radial distribution function $g(r)$ is applied in calculating the formation of the HBs.^{23,24,33} The first peak of $g(r)$ within $r = 2.0$ Å indicates HB formation, and the integrations of the $g(r) \times r^2$ function up to $r = 2.5$ Å are used to calculate the statistics of HBs in the first solvation shell.^{24,44} The HBs formed in the air-nanoparticle interface are compared with those formed inside the bulk nanoparticle. When DMA is placed in the air-nanoparticle interface, the four types of HBs are illustrated by the $g(r)$ s and the integrations of $g(r) \times r^2$ in Fig. 2a and 4b. Neither $H_{\text{DMA}} \cdots O_{\text{SA}}$ HB nor $H_{\text{DMA}} \cdots O_{\text{water}}$ HB is formed in the air-nanoparticle interface (the green area and the blue area in Fig. 2a) and their statistics are obtained as zero (the green line and the blue line in Fig. 2b). The

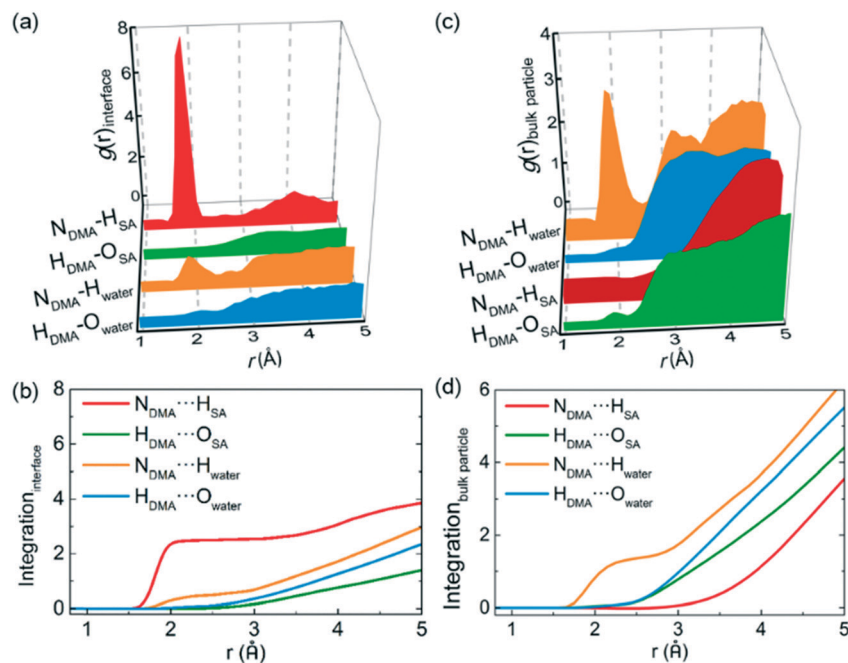


Fig. 2 The radial distribution function $g(r)$ s and the integrations of the HBs formed in the air-nanoparticle interface (Fig. 2a and b) and inside the bulk nanoparticle (Fig. 2c and d). The curves for the $N_{\text{DMA}} \cdots H_{\text{SA}}$ HB, $H_{\text{DMA}} \cdots O_{\text{SA}}$ HB, $N_{\text{DMA}} \cdots H_{\text{water}}$ HB and $H_{\text{DMA}} \cdots O_{\text{water}}$ HB are displayed as the red line, the green line, the orange line and the blue line, respectively.

formations of the $N_{\text{DMA}} \cdots H_{\text{SA}}$ HB and $N_{\text{DMA}} \cdots H_{\text{water}}$ HB are detected in the air–nanoparticle interface (the red area and the orange area in Fig. 2a). Accordingly, DMA can directly interact with SA and water in the air–nanoparticle interface. It is different from ammonia which only directly interacts with water. The statistics of $N_{\text{DMA}} \cdots H_{\text{SA}}$ HBs and $N_{\text{DMA}} \cdots H_{\text{water}}$ HBs are calculated to be 2.4 and 0.4, respectively (the red line and the orange line in Fig. 2b), indicating that the first solvation shell is composed of the mixture of SA and water in the air–nanoparticle interface. Moreover, the statistics of the $N_{\text{DMA}} \cdots H_{\text{SA}}$ HBs is six times that of the $N_{\text{DMA}} \cdots H_{\text{water}}$ HBs. This indicates that the direct interaction of DMA–SA more readily occurs than the direct interaction of DMA–water in the air–nanoparticle interface. This would promote the reaction of DMA–SA to proceed in the air–nanoparticle interface. Thus, this indicated that DMA would simultaneously react with interfacial SA and gaseous SA.

After DMA is moved into the bulk nanoparticle, the formations of the four types of HBs are then investigated by $g(r)$ and the integrations of $g(r) \times r^2$ as shown in Fig. 2c and d, respectively. The $N_{\text{DMA}} \cdots H_{\text{SA}}$, $H_{\text{DMA}} \cdots O_{\text{SA}}$ and $H_{\text{DMA}} \cdots O_{\text{water}}$ HBs are not formed inside the bulk nanoparticle (the red, green and blue areas in Fig. 2c), and their statistics are thereby obtained as zero. The $N_{\text{DMA}} \cdots H_{\text{water}}$ HB is detected inside the bulk nanoparticle (the orange area in Fig. 2c). Therefore, only the direct interactions of DMA–water occur inside the bulk nanoparticle. The statistics of the $N_{\text{DMA}} \cdots H_{\text{water}}$ HBs is found to be 1.1 inside the nanoparticle (the orange line in Fig. 2d), which is about three times that of the $N_{\text{DMA}} \cdots H_{\text{water}}$ HBs formed in the air–nanoparticle interface; the statistics of the $N_{\text{DMA}} \cdots H_{\text{SA}}$ HBs is zero inside the bulk nanoparticle, while the statistics of the $N_{\text{DMA}} \cdots H_{\text{SA}}$ HB is 2.4 in the air–nanoparticle interface. The changes in the statistics of the $N_{\text{DMA}} \cdots H_{\text{water}}$ HBs and $N_{\text{DMA}} \cdots H_{\text{SA}}$ HBs suggest that the first solvation shell is recomposed. The components of the first solvation shell change from the mixture of SA and water to only water as DMA is moved from the air–nanoparticle interface to inside the bulk nanoparticle. Inside the bulk nanoparticle, DMA is surrounded by the first solvation shell of water and is hindered from directly interacting with SA. Consequently, the nanoparticle is only stabilized but not promoted to a larger size by DMA inside the bulk nanoparticle.

To further identify the reaction of DMA–SA proceeding in the air–nanoparticle interface, the DMA–SA cluster was extracted from each MD configuration when DMA is placed in the air–nanoparticle interface (Fig. 3a). The DMA–SA cluster is composed of DMA and SA. Among the five hundred DMA–SA clusters, the most stable cluster is also re-optimized by the QM method and the relative results are shown in Fig. 3b. In the most stable DMA–SA cluster, the original length of the $N_{\text{DMA}} \cdots H_{\text{SA}}$ HB and $H_{\text{SA}} \cdots O_{\text{SA}}$ bond of SA is found to be 1.92 Å and 1.49 Å, respectively. After the reaction of DMA–SA in the air–nanoparticle interface, the proton of SA is transferred to the N of DMA. The $N_{\text{DMA}} \cdots H_{\text{SA}}$ bond (the red solid line) is formed with a length of 1.03 Å. The original $H_{\text{SA}} \cdots O_{\text{SA}}$ bond is broken, and the present distance between

H_{SA} and O_{SA} (the black dashed line) is stretched to 2.09 Å. As a result, dimethylammonium bisulfate is formed inside the nanoparticle. The recent field observation and laboratory measurements^{12,21,45} have identified the dimethylammonium bisulfate formed in the nanoparticle, but our results can also further confirm that dimethylammonium bisulfate is accumulated in the air–nanoparticle interface from the point of view of the theoretical calculations. This means that DMA will simultaneously react with aqueous SA in the interface and gaseous SA outside the nanoparticle. The reaction of DMA–SA will happen even though the concentration of gaseous SA is lower than the concentration of aqueous SA inside the bulk nanoparticle. Hence, the heterogeneous reaction of DMA–SA is independent from the concentration of SA as observed in the experimental work.¹⁶

3.3 The heterogeneous reactions in the ammonia–SA–water system

The stability of the ammonia–SA system was observed to be lower than that of DMA–SA–water present in the air–nanoparticle interface; thus the different heterogeneous reactions within the two systems were also comparably investigated in detail. To further clarify the difference in both heterogeneous reactions, four types of HBs formed in the ammonia–SA–water system, such as $N_{\text{ammonia}} \cdots H_{\text{SA}}$, $H_{\text{ammonia}} \cdots O_{\text{SA}}$, $N_{\text{ammonia}} \cdots H_{\text{water}}$ and $H_{\text{ammonia}} \cdots O_{\text{water}}$, are also analyzed. The $g(r)$ s and the integrations of $g(r) \times r^2$ of the HBs formed in the air–nanoparticle interface are shown in Fig. 4a and b, respectively. The $N_{\text{ammonia}} \cdots H_{\text{water}}$ HB in the air–nanoparticle interface is detected and shown in the orange area in Fig. 4a. The formation of the $H_{\text{ammonia}} \cdots O_{\text{water}}$ HB is not observed in the air–nanoparticle interface; however the H_{ammonia} atoms are surrounded by the interfacial O_{water} atoms since a shoulder appears at $r = 2.25$ Å (the blue area in Fig. 4a). Thus, the direct interactions of ammonia–water are proven to occur in the air–nanoparticle interface. The statistics of the $N_{\text{ammonia}} \cdots H_{\text{water}}$ HB is found to be 1.1 (the orange line in Fig. 4b), indicating that the first solvation shell is composed of water as ammonia is in the air–nanoparticle interface. No

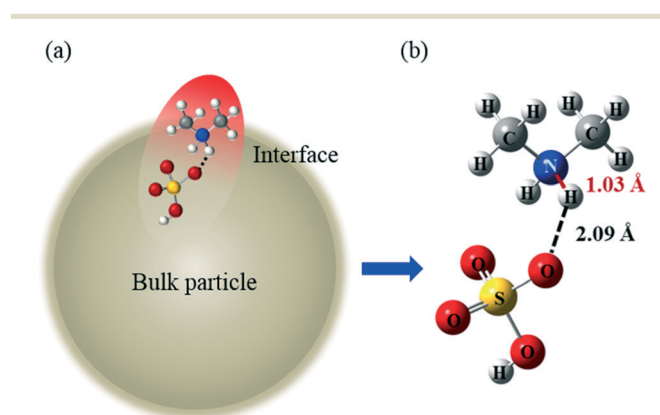


Fig. 3 (a) The MD configuration containing the DMA–SA cluster. (b) The re-optimized DMA–SA cluster by the QM method.

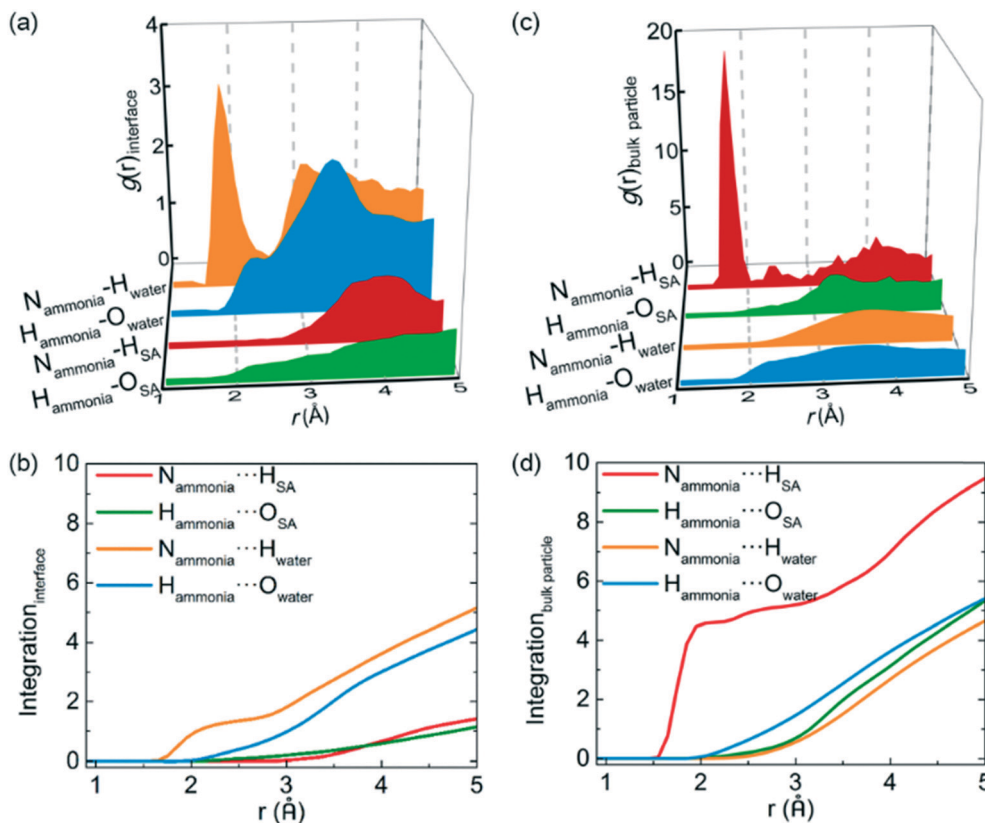


Fig. 4 The radial distribution function $g(r)$ s and the integrations of $g(r) \times r^2$ for the HBs formed in the air–nanoparticle interface (Fig. 4a and b) and inside the bulk nanoparticle (Fig. 4c and d). The curves for the $N_{\text{ammonia}} \cdots H_{\text{SA}}$ HB, $H_{\text{ammonia}} \cdots O_{\text{SA}}$ HB, $N_{\text{ammonia}} \cdots H_{\text{water}}$ HB and $H_{\text{ammonia}} \cdots O_{\text{water}}$ HB are shown as the red line, the green line, the orange line and the blue line, respectively.

$N_{\text{ammonia}} \cdots H_{\text{SA}}$ HB or $H_{\text{ammonia}} \cdots O_{\text{SA}}$ HB is detected (the red area and the green area in Fig. 4a), and their statistics are thereby obtained as zero (the red line and the green line Fig. 4b). The results imply that the direct interactions of ammonia–SA do not proceed in the air–nanoparticle interface. This is because the direct interaction of ammonia with SA is hindered by the first solvation shell composed of interfacial water. Therefore, the nanoparticle is only stabilized but not promoted to a larger size by ammonia in the air–nanoparticle interface.

The HBs formed inside the bulk nanoparticle are also analyzed by the $g(r)$ and the integrations of $g(r) \times r^2$ as shown in Fig. 4c and d. Neither the $N_{\text{ammonia}} \cdots H_{\text{water}}$ HB nor $H_{\text{ammonia}} \cdots O_{\text{water}}$ HB is observed inside the bulk nanoparticle (the orange area and the blue area in Fig. 4c), and their statistics are hence zero (the orange line and the blue line in Fig. 4d). Therefore, the direct interaction of ammonia–water is not proven inside the bulk nanoparticle. The $H_{\text{ammonia}} \cdots O_{\text{SA}}$ HB is not formed inside the bulk nanoparticle (the green area in Fig. 4c), and the statistics is zero (the green line in Fig. 4d). However, the $N_{\text{ammonia}} \cdots H_{\text{SA}}$ HB is detected inside the bulk nanoparticle (the red area in Fig. 4c). Hence, the direct interaction of ammonia–SA occurs inside the nanoparticle. The statistics of the $N_{\text{ammonia}} \cdots H_{\text{SA}}$ HBs formed inside the nanoparticle is calculated to be 4.5 (the red line in Fig. 4d) which is four times that of the $N_{\text{ammonia}} \cdots H_{\text{water}}$ HBs

formed in the air–nanoparticle interface. This means that the first solvation shell is recomposed of SA as ammonia is inside the bulk nanoparticle. Within the first solvation shell inside the bulk nanoparticle, the $N_{\text{ammonia}} \cdots H_{\text{SA}}$ HB would promote the proton transfer from SA to ammonia. Thus, the reaction of ammonia–SA is facilitated to proceed inside the bulk nanoparticle.

To further confirm the reaction of ammonia–SA occurring inside the bulk nanoparticle, the ammonia–SA cluster is also extracted from each MD configuration when ammonia is inside the bulk nanoparticle (Fig. 5a). The ammonia–SA cluster is composed of ammonia and SA directly interacting with

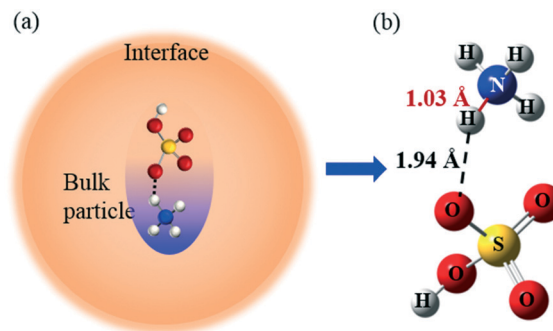


Fig. 5 (a) The MD configuration containing the ammonia–SA cluster. (b) The re-optimized ammonia–SA cluster by the QM method.

ammonia. Among the five hundred ammonia-SA clusters, the most stable cluster is re-optimized by the QM method and the results are shown in Fig. 5b. The length of the original $N_{\text{ammonia}}\cdots H_{\text{SA}}$ HB and $H_{\text{SA}}\cdots O_{\text{SA}}$ bond of SA is found to be 1.72 Å and 0.97 Å, respectively. After the reaction of ammonia-SA inside the bulk nanoparticle, the proton bonded to SA is transferred to the N of ammonia. The $N_{\text{ammonia}}\cdots H_{\text{SA}}$ bond (the red solid line) is formed with a length of 1.03 Å. Meanwhile, the original $H_{\text{SA}}\cdots O_{\text{SA}}$ bond (the black dashed line) is broken. The distance between H_{SA} and O_{SA} is stretched to 1.94 Å. As a result, ammonium bisulfate is formed inside the bulk nanoparticle. The reaction of ammonia-SA is also verified by Kurtén *et al.*'s¹³ and Henschel *et al.*'s⁴⁶ calculated results; however our results further revealed that the reaction proceeds inside the bulk nanoparticle. This explains why the aqueous SA inside the nanoparticle is the only source to react with ammonia. The diffusion of gaseous SA is driven by the gradient in the SA concentration. Consequently, the higher concentration of gaseous SA than that of aqueous SA is a necessary condition to make the interface reaction of ammonia-SA happen. It can well explain the phenomenon observed in the experiments where the growth of the nanoparticle exposed to ammonia relies on the concentration of gaseous SA.^{14,15}

3.4 The environmental implications on the growth of atmospheric nanoparticles

During the growth of a fresh nanoparticle, the SA concentration inside the bulk nanoparticle rises as the nanoparticle grows during the new particle formation events.¹⁶ The SA concentration used in our work is 59 wt% which is considered as a high level occurring in a concentrated nanoparticle.¹⁶ To further identify whether DMA promotes the growth of a less concentrated nanoparticle, another two DMA-SA-water systems with lower SA concentration are also constructed and compared with the above system. The SA concentrations of the two systems are selected to be 20 wt% and 40 wt%, respectively. The free energy profiles of the two diluted modes of 20 wt% SA and 40 wt% SA were also calculated. As illustrated in Fig. 6, the free energy profiles of the two diluted DMA-SA-water systems are compared with the 59 wt% SA system. The free energy difference from point c-2 to point c-3 is calculated to be 2.7 kcal mol⁻¹ for the 20 wt% SA system and 2.2 kcal mol⁻¹ for the 40 wt% SA system, respectively. The free energy difference is comparable to 2.9 kcal mol⁻¹ for the 59 wt% SA system. This implies that the heterogeneous reactions of DMA with solutes also more readily proceed in the air-nanoparticle interface of the less concentrated nanoparticles. In order to confirm the heterogeneous reactions proceeding in the interface of the less concentrated nanoparticles, the HBs formed in the 20 wt% SA-system and 40 wt% SA-system are further analyzed by RDFs in Fig. S5 and S6.† In the 20 wt% SA-system, as shown in Fig. S5a,† $H_{\text{DMA}}\cdots O_{\text{SA}}$, $H_{\text{DMA}}\cdots O_{\text{water}}$ and $H_{\text{DMA}}\cdots O_{\text{water}}$ HBs are detected. Within the distance of 2.5 Å to DMA, their coordi-

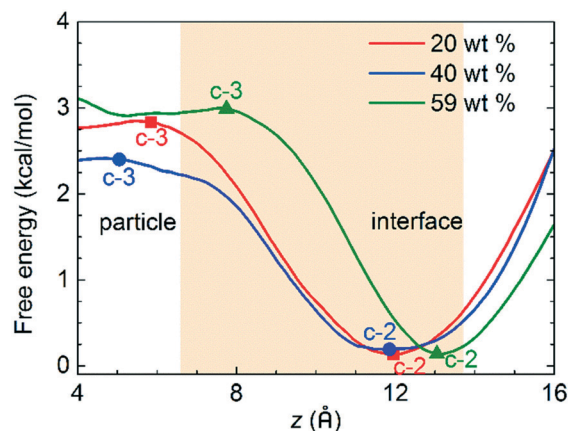


Fig. 6 Free energy profile of DMA varying with different SA concentrations.

nation numbers are 0.2, 0.7 and 2.2. The $N_{\text{DMA}}\cdots H_{\text{SA}}$ HB is not formed (Fig. S5b†). Thus, in the 20 wt% SA-system, the first solution shell is mainly composed of water molecules with a few SA molecules in the air-nanoparticle interface. In contrast, in the interface of the 59 wt% SA-system, the first solution shell is mainly composed of SA molecules with a few water molecules. Hence, the heterogeneous reactions of DMA-SA less efficiently proceed in the 20 wt% SA-system than in the 59 wt% SA-system. In the 40 wt% SA-system, as displayed in Fig. S6a,† $N_{\text{DMA}}\cdots H_{\text{SA}}$, $H_{\text{DMA}}\cdots O_{\text{SA}}$, $H_{\text{DMA}}\cdots O_{\text{water}}$ and $H_{\text{DMA}}\cdots O_{\text{water}}$ HBs are all formed in the air-nanoparticle interface. In particular, the peak of the $N_{\text{DMA}}\cdots H_{\text{SA}}$ HB is obviously higher than any other peak of the other HBs, implying the strong interaction of DMA with SA. The coordination numbers are 1.5, 0.1, 0.6 and 0.9 for $N_{\text{DMA}}\cdots H_{\text{SA}}$, $H_{\text{DMA}}\cdots O_{\text{SA}}$, $H_{\text{DMA}}\cdots O_{\text{water}}$ and $H_{\text{DMA}}\cdots O_{\text{water}}$ HBs, respectively (Fig. S6b†). Hereby, the first shell is composed of more SA molecules than water molecules. This indicates that the DMA-SA reactions more efficiently occur than DMA-water reactions in the 40 wt% SA system. Hence, DMA possibly promotes the growth of the less concentrated nanoparticles. The SA concentration rises as the nanoparticle grows, and further inhibits the diffusion of gaseous SA into the bulk nanoparticle. Therefore, the reaction of ammonia-SA is hindered inside the bulk nanoparticle. The reaction of DMA-SA is found to be independent from the concentration of gaseous SA; hence the reaction of DMA-SA could sustainably proceed in the air-nanoparticle interface. As a result, DMA becomes more competitive in promoting the nanoparticle growth than ammonia as the acidity is gradually concentrated. It is speculated that DMA would promote the sustainable growth of the nanoparticle during the NPF events where the acidity of the nanoparticle is concentrated.

Our above results clarified that the heterogeneous reaction of DMA is different from that of ammonia in promoting the growth of the nanoparticle. In the DMA-SA-water system, the first solvation shell is composed of SA and water around DMA in the air-nanoparticle interface as shown in the green circle in Fig. 7a. After DMA is dissolved inside the bulk

nanoparticle, the first solvation shell is recomposed of water as shown in the blue circle in Fig. 7a. Thus, the cluster of DMA-SA is favored to form in the air-nanoparticle interface (Fig. 7b). For the concentrated nanoparticle, gaseous SA is difficult to diffuse into the bulk nanoparticle because the aqueous SA concentration in the concentrated nanoparticle is higher than that of gaseous SA in the air. Nevertheless, DMA can directly capture gaseous SA approaching the air-nanoparticle interface. Thus, DMA will simultaneously react with gaseous and aqueous SA, which ensures that the reaction of DMA-SA efficiently proceeds in the concentrated nanoparticle. But, in the ammonia-SA-water system, the first solvation shell is composed of interfacial water as ammonia occurs in the air-nanoparticle interface (the blue circle in Fig. 7c). This inhibits the formation of the ammonia-SA cluster in the air-nanoparticle interface. After ammonia is moved into the bulk nanoparticle, the first shell is recomposed of SA (the green circle in Fig. 7c). The formation of the ammonia-SA cluster is subsequently confirmed inside the bulk nanoparticle (Fig. 7d). The diffusions of gaseous SA are driven by the gradient in the SA concentration; therefore the lower SA concentration inside the bulk nanoparticle than that in the air is a necessary condition for the reaction of ammonia-SA. Accordingly, it is not likely that ammonia will promote the growth of the concentrated nanoparticle.

As amines and ammonia are two kinds of strong bases that neutralize SA in the atmosphere, it is believed that there

is a competitive relationship between them. This work stated that the ammonia-SA reactions more efficiently occur in the fresh nanoparticle. Moreover, the concentration of ammonia is 2–3 orders of magnitude higher than that of DMA in the atmosphere.¹³ Hence, it is plausible that the ammonia-SA reaction is more competitive than the DMA-SA reaction on the fresh nanoparticle. This conclusion is also confirmed by the experimental work which confirms that the heterogeneous uptake coefficient of ammonia is larger than that of amines.¹⁶ Accordingly, the growth of the fresh nanoparticle is more promoted by ammonia. In the NPF event, the fresh nanoparticle becomes concentrated with a higher SA concentration inside. Based on Qiu *et al.*'s work, the displacement reaction between amines and ammonium is irreversible.⁴⁷ It is also verified that the displacement would completely finish within a few seconds in sub-3 nm nanoparticles. Hereby, under enough DMA source, DMA-SA reactions will efficiently proceed in the concentrated nanoparticle. The growth of the concentrated nanoparticle is promoted by DMA after a quick displacement reaction between DMA and ammonium.

4. Conclusions

The heterogeneous reaction of dimethylamine/ammonia with sulfuric acid to promote the growth of atmospheric nanoparticles was investigated in detail in this work. Complementary to experimental methods, the combined theoretical methods of MD and QM were applied to compare the heterogeneous reactions of DMA and ammonia in the air-nanoparticle interface as well as inside the bulk nanoparticle. The results verified that the interface reaction mechanism of DMA in promoting atmospheric nanoparticle growth is different from that of ammonia. DMA more easily approaches the air-nanoparticle interface than ammonia, thus it is more likely that the interface heterogeneous reaction of DMA with SA will occur than that of ammonia. In the DMA-SA-water system, the DMA-SA cluster is formed within the first solvation shell in the air-nanoparticle interface. This indicates that the reaction of DMA with SA is independent from the concentration of gaseous SA in the atmosphere. In contrast, in the ammonia-SA-water system, the ammonia-SA cluster readily forms inside the bulk particle. Thereby, the reaction of ammonia with SA is dependent on the concentration of atmospheric SA. The difference in the mechanism of the heterogeneous reaction of DMA and ammonia with SA further results in DMA being more competitive than ammonia in promoting the growth of the concentrated nanoparticle. However, considering the 2–3 orders of magnitude higher concentration of ammonia than that of DMA in the atmosphere,¹³ ammonia more efficiently promotes the growth of the fresh nanoparticle than DMA. The results of the two diluted models constructed to explain why DMA would promote the sustainable growth of the nanoparticle during the NPF events where the acidity of the nanoparticle is concentrated are also reported.

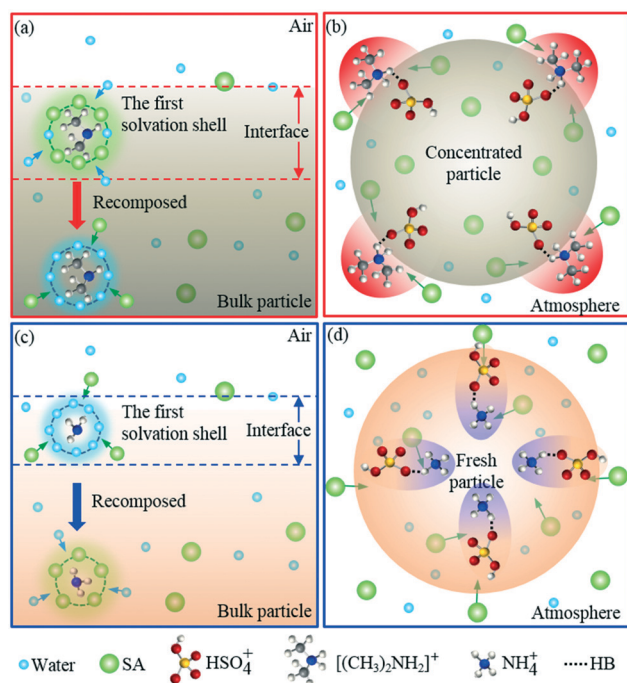


Fig. 7 Difference in the mechanism of DMA and ammonia in promoting the growth of atmospheric nanoparticles. (a) The first solvation shell formed in the DMA-SA-water system. (b) DMA-SA reaction occurring in the air-nanoparticle interface. (c) The first solvation shell formed in the ammonia-SA-water system. (d) Ammonia-SA reaction occurring inside the bulk nanoparticle.

Conflicts of interest

There are no conflicts to declare.

Acknowledgements

This research was financially supported by the National Natural Science Foundation of China (41425015, 41675122 and 41731279), the Local Innovative and Research Team Project of Guangdong Pearl River Talents Program (2017BT01Z032), the Innovation Team Project of Guangdong Provincial Department of Education (2017KCXTD012), the Leading Scientific, Technical and Innovation Talents of Guangdong Special Support Program (2016TX03Z094), the China Postdoctoral Science Foundation Grant (2018M633016), and the Science and Technology Program of Guangzhou City (201707010188).

Notes and references

- 1 A. Virtanen, J. Joutsensaari, T. Koop, J. Kannosto, P. Yli-Pirila, J. Leskinen, J. M. Makela, J. K. Holopainen, U. Poschl, M. Kulmala, D. R. Worsnop and A. Laaksonen, *Nature*, 2010, **467**, 824–827.
- 2 R. J. Huang, Y. Zhang, C. Bozzetti, K. F. Ho, J. J. Cao, Y. Han, K. R. Daellenbach, J. G. Slowik, S. M. Platt, F. Canonaco, P. Zotter, R. Wolf, S. M. Pieber, E. A. Brunns, M. Crippa, G. Ciarelli, A. Piazzalunga, M. Schwikowski, G. Abbazade, J. Schnelle-Kreis, R. Zimmermann, Z. An, S. Szidat, U. Baltensperger, I. El Haddad and A. S. Prevot, *Nature*, 2014, **514**, 218–222.
- 3 P. Zhang, D. Y. Wan, Z. Y. Zhang, G. D. Wang, J. H. Hu and G. S. Shao, *Environ. Sci.: Nano*, 2018, **5**, 1813–1820.
- 4 M. Kulmala, J. Kontkanen, H. Junninen, K. Lehtipalo, H. E. Manninen, T. Nieminen, T. Petaja, M. Sipila, S. Schobesberger, P. Rantala, A. Franchin, T. Jokinen, E. Jarvinen, M. Aijala, J. Kangasluoma, J. Hakala, P. P. Aalto, P. Paasonen, J. Mikkila, J. Vanhanen, J. Aalto, H. Hakola, U. Makkonen, T. Ruuskanen, R. L. Mauldin, 3rd, J. Duplissy, H. Vehkamäki, J. Back, A. Kortelainen, I. Riipinen, T. Kurten, M. V. Johnston, J. N. Smith, M. Ehn, T. F. Mentel, K. E. Lehtinen, A. Laaksonen, V. M. Kerminen and D. R. Worsnop, *Science*, 2013, **339**, 943–946.
- 5 M. Sipilä, T. Berndt, T. Petäjä, D. Brus, J. Vanhanen, F. Stratmann, J. Patokoski, R. L. M. III, A.-P. Hyvärinen, H. Lihavainen and M. Kulmala, *Science*, 2010, **327**, 1243–1245.
- 6 M. Boy, M. Kulmala, T. M. Ruuskanen, M. Pihlatie, A. Reissell, P. P. Aalto, P. Keronen, M. D. Maso, H. Hellen, H. Hakola, R. Jansson, M. Hanke and F. Arnold, *Atmos. Chem. Phys.*, 2005, **5**, 863–878.
- 7 D. Brus, A.-P. Hyvärinen, Y. Viisanen, M. Kulmala and H. Lihavainen, *Atmos. Chem. Phys.*, 2010, **10**, 2631–2641.
- 8 R. Zhang, I. Suh, J. Zhao, D. Zhang and E. C. Fortner, *Science*, 2004, **304**, 1487–1490.
- 9 J. Merikanto, I. Napari, H. Vehkamäki, T. Anttila and M. Kulmala, *J. Geophys. Res.*, 2007, **112**, D15207.
- 10 J. Almeida, S. Schobesberger, A. Kurten, I. K. Ortega, O. Kupiainen-Maatta, A. P. Praplan, A. Adamov, A. Amorim, F. Bianchi, M. Breitenlechner, A. David, J. Dommen, N. M. Donahue, A. Downard, E. Dunne, J. Duplissy, S. Ehrhart, R. C. Flagan, A. Franchin, R. Guida, J. Hakala, A. Hansel, M. Heinritzi, H. Henschel, T. Jokinen, H. Junninen, M. Kajos, J. Kangasluoma, H. Keskinen, A. Kupc, T. Kurten, A. N. Kvashin, A. Laaksonen, K. Lehtipalo, M. Leiminger, J. Leppa, V. Loukonen, V. Makhmutov, S. Mathot, M. J. McGrath, T. Nieminen, T. Olenius, A. Onnela, T. Petaja, F. Riccobono, I. Riipinen, M. Rissanen, L. Rondo, T. Ruuskanen, F. D. Santos, N. Sarnela, S. Schallhart, R. Schnitzhofer, J. H. Seinfeld, M. Simon, M. Sipila, Y. Stozhkov, F. Stratmann, A. Tome, J. Trostl, G. Tsagkogeorgas, P. Vaattovaara, Y. Viisanen, A. Virtanen, A. Vrtala, P. E. Wagner, E. Weingartner, H. Wex, C. Williamson, D. Wimmer, P. Ye, T. Yli-Juuti, K. S. Carslaw, M. Kulmala, J. Curtius, U. Baltensperger, D. R. Worsnop, H. Vehkamäki and J. Kirkby, *Nature*, 2013, **502**, 359–363.
- 11 J. S. Youn, E. Crosbie, L. C. Maudlin, Z. Wang and A. Sorooshian, *Atmos. Environ.*, 2015, **122**, 250–258.
- 12 L. Yao, O. Garmash, F. Bianchi, J. Zheng, C. Yan, J. Kontkanen, H. Junninen, S. B. Mazon, M. Ehn, P. Paasonen, M. Sipilä, M. Wang, X. Wang, S. Xiao, H. Chen, Y. Lu, B. Zhang, D. Wang, Q. Fu, F. Geng, L. Li, H. Wang, L. Qiao, X. Yang, J. Chen, V.-M. Kerminen, T. Petaja, D. R. Worsnop, M. Kulmala and L. Wang, *Science*, 2018, **361**, 278–281.
- 13 T. Kurtén, V. Loukonen, H. Vehkamäki and M. Kulmala, *Atmos. Chem. Phys.*, 2008, **8**, 4095–4103.
- 14 G. Biskos, P. R. Buseck and S. T. Martin, *J. Aerosol Sci.*, 2009, **40**, 338–347.
- 15 R. Zhang, L. Wang, A. F. Khalizov, J. Zhao, J. Zheng, R. L. McGraw and L. T. Molina, *Proc. Natl. Acad. Sci. U. S. A.*, 2009, **106**, 17650–17654.
- 16 L. Wang, V. Lal, A. F. Khalizov and R. Zhang, *Environ. Sci. Technol.*, 2010, **44**, 2461–2465.
- 17 R. Zhang, A. Khalizov, L. Wang, M. Hu and W. Xu, *Chem. Rev.*, 2012, **112**, 1957–2011.
- 18 K. Li, L. Kong, A. Zhanzakova, S. Tong, J. Shen, T. Wang, L. Chen, Q. Li, H. Fu and L. Zhang, *Environ. Sci.: Nano*, 2019, **6**, 1838–1851.
- 19 A. Kuerten, T. Jokinen, M. Simon, M. Sipilä, N. Sarnela, H. Junninen, A. Adamov, J. Almeida, A. Amorim, F. Bianchi, M. Breitenlechner, J. Dommen, N. M. Donahue, J. Duplissy, S. Ehrhart, R. C. Flagan, A. Franchin, J. Hakala, A. Hansel, M. Heinritzi, M. Hutterli, J. Kangasluoma, J. Kirkby, A. Laaksonen, K. Lehtipalo, M. Leiminger, V. Makhmutov, S. Mathot, A. Onnela, T. Petaja, A. P. Praplan, F. Riccobono, M. P. Rissanen, L. Rondo, S. Schobesberger, J. H. Seinfeld, G. Steiner, A. Tome, J. Troestl, P. M. Winkler, C. Williamson, D. Wimmer, P. Ye, U. Baltensperger, K. S. Carslaw, M. Kulmala, D. R. Worsnop and J. Curtius, *Proc. Natl. Acad. Sci. U. S. A.*, 2014, **111**, 15019–15024.
- 20 P. Paasonen, T. Olenius, O. Kupiainen, T. Kurten, T. Petaja, W. Birmili, A. Hamed, M. Hu, L. G. Huey, C. Plass-Duelmer, J. N. Smith, A. Wiedensohler, V. Loukonen, M. J. McGrath, I. K. Ortega, A. Laaksonen, H. Vehkamäki, V. M. Kerminen and M. Kulmala, *Atmos. Chem. Phys.*, 2012, **12**, 9113–9133.
- 21 C. N. Jen, P. H. McMurry and D. R. Hanson, *J. Geophys. Res.: Atmos.*, 2014, **119**, 7502–7514.

- 22 J. Kirkby, J. Curtius, J. Almeida, E. Dunne, J. Duplissy, S. Ehrhart, A. Franchin, S. Gagné, L. Ickes, A. Kürten, A. Kupe, A. Metzger, F. Riccobono, L. Rondo, S. Schobesberger, G. Tsagkogeorgas, D. Wimmer, A. Amorim, F. Bianchi, M. Breitenlechner, A. David, J. Dommen, A. Downard, M. Ehn, R. C. Flagan, S. Haider, A. Hansel, D. Hauser, W. Jud, H. Junninen, F. Kreissl, A. Kvashin, A. Laaksonen, K. Lehtipalo, J. Lima, E. R. Lovejoy, V. Makhmutov, S. Mathot, J. Mikkilä, P. Minginette, S. Mogo, T. Nieminen, A. Onnela, P. Pereira, T. Petäjä, R. Schnitzhofer, J. H. Seinfeld, M. Sipilä, Y. Stozhkov, F. Stratmann, A. Tomé, J. Vanhanen, Y. Viisanen, A. Vrtala, P. E. Wagner, H. Walther, E. Weingartner, H. Wex, P. M. Winkler, K. S. Carslaw, D. R. Worsnop, U. Baltensperger and M. Kulmala, *Nature*, 2011, **476**, 429–433.
- 23 J. Zhong, M. Kumar, J. S. Francisco and X. C. Zeng, *Acc. Chem. Res.*, 2018, **51**, 1229–1237.
- 24 M. T. C. Martins-Costa, J. M. Anglada, J. S. Francisco and M. F. Ruiz-Lopez, *J. Am. Chem. Soc.*, 2012, **134**, 11821–11827.
- 25 J. Zhong, M. Kumar, C. Q. Zhu, J. S. Francisco and X. C. Zeng, *Angew. Chem., Int. Ed.*, 2017, **56**, 7740–7744.
- 26 Y. Liu, Q. Ma and H. He, *Environ. Sci. Technol.*, 2012, **46**, 11112–11118.
- 27 D. R. Benson, J. H. Yu, A. Markovich and S. H. Lee, *Atmos. Chem. Phys.*, 2011, **11**, 4755–4766.
- 28 Y. Wang, J. Comer, Z. F. Chen, J. W. Chen and J. C. Gumbart, *Environ. Sci.: Nano*, 2018, **5**, 2117–2128.
- 29 J. A. Riddick, W. B. Bunger and T. K. Sakano, *Organic solvents physical properties and methods of purification (techniques of chemistry)*, Wiley-Interscience, 1970.
- 30 M. T. Martins-Costa and M. F. Ruiz-Lopez, *Phys. Chem. Chem. Phys.*, 2011, **13**, 11579–11582.
- 31 H. Uslu, D. Datta and H. S. Bamufleh, *Ind. Eng. Chem. Res.*, 2016, **55**, 3659–3667.
- 32 J. Yoo and A. Aksimentiev, *Biophys. J.*, 2016, **110**, 646A.
- 33 X. Yang, R. J. Rees, W. Conway, G. Puxty, Q. Yang and D. A. Winkler, *Chem. Rev.*, 2017, **117**, 9524–9593.
- 34 J. C. Phillips, R. Brau, W. Wang, J. Gumbart, E. Tajkhorshid, E. Villa, C. Chipot, R. D. Skeel, L. Kale and K. Schulten, *J. Comput. Chem.*, 2005, **26**, 1781–1802.
- 35 W. Humphrey, A. Dalke and K. Schulten, *J. Mol. Graphics*, 1996, **14**, 33–38.
- 36 G. M. Torrie and J. P. Valleau, *J. Comput. Phys.*, 1997, **23**, 187.
- 37 B. Roux, *Comput. Phys. Commun.*, 1995, **91**, 275–282.
- 38 S. Kumar, J. M. Rosenberg, D. Bouzida, R. H. Swendsen and P. Kollman, *J. Comput. Chem.*, 1995, **16**, 1339–1350.
- 39 Y. Ji, J. Zhao, H. Terazono, K. Misawa, N. P. Levitt, Y. Li, Y. Lin, J. Peng, Y. Wang, L. Duan, B. Pan, F. Zhang, X. Feng, T. An, W. Marrero-Ortiz, J. Secrest, A. L. Zhang, K. Shibuya, M. J. Molina and R. Zhang, *Proc. Natl. Acad. Sci. U. S. A.*, 2017, **114**, 8169–8174.
- 40 H. B. Xie, C. Li, N. He, C. Wang, S. Zhang and J. Chen, *Environ. Sci. Technol.*, 2014, **48**, 1700–1706.
- 41 M. J. Frisch, G. W. Trucks, H. B. Schlegel, G. E. Scuseria, M. A. Robb, J. R. Cheeseman, G. Scalmani, V. Barone, B. Mennucci, G. A. Petersson, H. Nakatsuji, M. Caricato, X. Li, H. P. Hratchian, A. F. Izmaylov, J. Bloino, G. Zheng, J. L. Sonnenberg, M. Hada, M. Ehara, K. Toyota, R. Fukuda, J. Hasegawa, M. Ishida, T. Nakajima, Y. Honda, O. Kitao, H. Nakai, T. Vreven, J. A. Montgomery, Jr., J. E. Peralta, F. Ogliaro, M. Bearpark, J. J. Heyd, E. Brothers, K. N. Kudin, V. N. Staroverov, T. Keith, R. Kobayashi, J. Normand, K. Raghavachari, A. Rendell, J. C. Burant, S. S. Iyengar, J. Tomasi, M. Cossi, N. Rega, J. M. Millam, M. Klene, J. E. Knox, J. B. Cross, V. Bakken, C. Adamo, J. Jaramillo, R. Gomperts, R. E. Stratmann, O. Yazyev, A. J. Austin, R. Cammi, C. Pomelli, J. W. Ochterski, R. L. Martin, K. Morokuma, V. G. Zakrzewski, G. A. Voth, P. Salvador, J. J. Dannenberg, S. Dapprich, A. D. Daniels, O. Farkas, J. B. Foresman, J. V. Ortiz, J. Cioslowski and D. J. Fox, *Gaussian 09, Revision D.01*, Gaussian, Inc., Wallingford CT, 2013.
- 42 M. T. C. Martins-Costa, F. F. García-Prieto and M. F. Ruiz-López, *Org. Biomol. Chem.*, 2015, **13**, 1673.
- 43 C. Zhu, M. Kumar, J. Zhong, L. Li, J. S. Francisco and X. C. Zeng, *J. Am. Chem. Soc.*, 2016, **138**, 11164–11169.
- 44 H. S. Ashbaugh, L. R. Pratt, M. E. Paulaitis, J. Clohery and T. L. Beck, *J. Am. Chem. Soc.*, 2005, **127**, 2808–2809.
- 45 B. R. Bzdek, D. P. Ridge and M. V. Johnston, *Atmos. Chem. Phys.*, 2011, **11**, 8735–8743.
- 46 H. Henschel, T. Kurten and H. Vehkamäki, *J. Phys. Chem. A*, 2016, **120**, 1886–1896.
- 47 C. Qiu, L. Wang and V. Lal, *Environ. Sci. Technol.*, 2011, **45**, 4748–4755.